

EVEN-ODD CYCLED HIGH-ORDER SPLITTING FINITE DIFFERENCE TIME DOMAIN METHOD FOR MAXWELL'S EQUATIONS

MANINDER SARAI AND DONG LIANG*

Abstract. In the paper, an even-odd cycled high-order splitting finite difference time domain scheme for Maxwell's equations in two dimensions is developed. The scheme uses fourth order spatial difference operators and even-odd time step technique to make it more accurate in both space and time. The scheme is energy-conserved, unconditionally stable and efficient in computation. We analyze in detail the stability, dispersion and phase error for the scheme. We prove that the scheme is energy conservative. Numerical experiments show numerically the energy conservation, high accuracy, and the divergence free accuracy. Furthermore, the developed scheme is applied to compute of the grounded coplanar waveguides.

Key words. Maxwell's Equations, even-odd cycled, high order in time, dispersion analysis, energy conservation, grounded coplanar waveguide.

1. Introduction

Maxwell's equations are widely used in computational electromagnetism applications such as, radio frequency, microwave, antennas, and air-craft radars and so on. Several ADI and splitting finite difference time domain methods have been developed to compute the solutions of Maxwell's equations. Second order schemes are commonly used for moderate numerical results, however, high order accuracy is more important in large scale applications. When computing modern problems of long distance wave propagations and moderately high frequency propagations, there are great interests to develop time and spatial high-order and energy-preserving schemes.

Finite difference time domain method (FDTD) for Maxwell's equations was first introduced by Yee [17] in 1966 which was further developed by other researchers [12,14] to a very efficient numerical algorithm in computational electromagnetics. However, the FDTD method is only conditionally stable and has large computational costs. Papers [13,19] proposed ADI-FDTD schemes for Maxwell's equations which are unconditionally stable and of second order accuracy. Papers [1,2] proposed energy-conserved spatial second-order S-FDTD schemes for Maxwell's equations which are efficient. The schemes are energy conserved, unconditionally stable and non-dissipative. Papers [7,8] developed energy-conserved spatial second-order S-FDTD schemes for metamaterial electromagnetics. Paper [9] developed a spatial fourth order energy-conserved S-FDTD schemes, EC-S-FDTD(1,4) and EC-S-FDTD(2,4), for Maxwell's equations, which are fourth order accurate in space.

In this paper, we develop an even-odd cycled energy-conserved splitting finite difference time domain scheme for solving Maxwell's equations in two dimensions, Even-Odd cycled 4th order EC-S-FDTD, shorten to the EO-4th-EC scheme, with fourth order accuracy in space and second order accuracy in time. For EO-4th-EC

Received by the editors December 5, 2020.

2000 *Mathematics Subject Classification.* 65N06, 65N12, 65M06, 65Y05.

*Corresponding author: Dong Liang; E-mail: dliang@yorku.ca.

scheme, we apply the spatial fourth order difference operators to a two stage splitting technique for each time step. The scheme consists of odd and even time step where for the odd time step, electric field in y -direction E_y and the intermediate value of magnetic field H_z are computed in stage one, following that electric field in x -direction E_x and H_z are solved in stage two. For the even time step, E_x and intermediate value H_z are computed in stage one and E_y and H_z are computed in stage 2. In this scheme, the spatial fourth order difference operators are obtained by a linear combination of two central differences on with a spatial step and one with three spatial steps while the boundary node difference operators are carefully defined keeping in mind the energy conservation and fourth order accuracy in space. Another important feature is that the use of even-odd two cycles achieves high-order accuracy in time while only using two stages in EO-4th-EC. We analyze in detail the stability, dispersion and phase error for the scheme. We also prove the scheme to be energy conservative. To find the stability of the scheme, the equivalent expressions for the even and odd time steps are computed by eliminating the intermediate terms. The expressions further allow us to compute the growth factor for each time step and the scheme overall. The growth factors help to determine the dispersion relationships of our scheme at each time step. The paper further focuses on numerical tests of the scheme. The phase velocity error of the proposed scheme are compared and computed with those other schemes such as ADI-FDTD, CN, EC-S-FDTD, EC-S-FDTDII and EC-S-FDTD (2,4). The energy conservation, accuracy errors and the divergence free approximations are computed and compared to other schemes as well. Overall, the proposed scheme is found to be unconditionally stable and non-dissipative. The scheme also conserves energy and has higher accuracy.

This high order scheme is finally used in applications of MMIC such as coplanar waveguides. Coplanar waveguide, CPW, is made of two parallel plates made of conducting material, such as copper or gold, that run with some dielectric materials in between. In the numerical experiments, two lumped ports are attached on top of a grounded CPW to excite the waveguide. It is shown that the electric wave produced from the lumped ports is strong in the metal and weakens as it travels through the dielectric material. The dielectric substrate is made thick enough that the EM wave dies out before it reaches the conductor at the bottom of the GCPW. We also analyze the wave propagation of an electric wave in a transition between a CPW and a rectangular waveguide. This transition consists of back to back CPW and rectangular waveguide made of linearized array of via holes. The transition is excited with a magnetic source at the center of the domain. As the magnetic wave moves outwards it changes its shape as it moves into a different material.

2. Model and Scheme

2.1. Maxwell's Equations in 2D. Consider the 2D transverse electric polarization case in a lossless medium and there is no source. We have

$$(1) \quad \frac{\partial E_x}{\partial t} = \frac{1}{\epsilon} \frac{\partial H_z}{\partial y},$$

$$(2) \quad \frac{\partial E_y}{\partial t} = -\frac{1}{\epsilon} \frac{\partial H_z}{\partial x},$$

$$(3) \quad \frac{\partial H_z}{\partial t} = \frac{1}{\mu} \left(\frac{\partial E_x}{\partial y} - \frac{\partial E_y}{\partial x} \right),$$

where ϵ and μ are the permittivity and permeability, $E = (E_x(x, y, t), E_y(x, y, t))$ is the electric field and $H_z = H_z(x, y, t)$ is the magnetic field for $(x, y) \in \Omega = (0, a) \times (0, b)$ and $t \in (0, T]$. Perfectly conducting boundary condition is satisfied on the boundary: $(E, 0) \times (\vec{n}, 0) = 0$ on $(0, T] \times \partial\Omega$, where $\partial\Omega$ is the boundary of Ω and \vec{n} is the outward normal vector on $\partial\Omega$. The initial conditions are $\mathbf{E}(x, y, 0) = \mathbf{E}_0(x, y) = (E_{x_0}(x, y), E_{y_0}(x, y))$, $H_z(x, y, 0) = H_{z_0}(x, y)$.

Let the partition of space domain Ω and the time interval $[0, T]$ be uniformly staggered grid:

$$\begin{aligned} x_i &= i\Delta x, x_{i+\frac{1}{2}} = x_i + \frac{1}{2}\Delta x, i = 0, 1, \dots, I-1, x_I = I\Delta x, \\ y_j &= j\Delta y, y_{j+\frac{1}{2}} = y_j + \frac{1}{2}\Delta y, j = 0, 1, \dots, J-1, y_J = J\Delta y, \\ t^n &= n\Delta t, t^{n+\frac{1}{2}} = t^n + \frac{1}{2}\Delta t, n = 0, 1, \dots, N-1, t^N = N\Delta t, \end{aligned}$$

where Δx and Δy are the mesh sizes along the x and y directions respectively, and Δt is the time step size, and I, J and N are integers. For a function $F(t, x, y)$, we let $F_{\alpha, \beta}^m = F(m\Delta t, \alpha\Delta x, \beta\Delta y)$, and define

$$\begin{aligned} \delta_t F_{\alpha, \beta}^m &= \frac{F_{\alpha, \beta}^{m+\frac{1}{2}} - F_{\alpha, \beta}^{m-\frac{1}{2}}}{\Delta t}, \\ \delta_x F_{\alpha, \beta}^m &= \frac{F_{\alpha+\frac{1}{2}, \beta}^m - F_{\alpha-\frac{1}{2}, \beta}^m}{\Delta x}, \\ \delta_y F_{\alpha, \beta}^m &= \frac{F_{\alpha, \beta+\frac{1}{2}}^m - F_{\alpha, \beta-\frac{1}{2}}^m}{\Delta y}, \\ \delta_u \delta_v F_{\alpha, \beta}^m &= \delta_u(\delta_v F_{\alpha, \beta}^m), u, v = x, y. \end{aligned}$$

For the strict interior nodes, we further define the fourth order difference operator to $\frac{\partial E_y}{\partial x}(x_{i+\frac{1}{2}}, y_{j+\frac{1}{2}})$ by

$$\Lambda_x E_{y_{i+\frac{1}{2}, j+\frac{1}{2}}}^n = \frac{1}{8}(9\delta_x - \delta_{2,x})E_{y_{i+\frac{1}{2}, j+\frac{1}{2}}}^n,$$

where

$$\delta_{2,x} E_{y_{\alpha, \beta}}^n = \frac{E_{y_{\alpha+\frac{3}{2}, \beta}}^n - E_{y_{\alpha-\frac{3}{2}, \beta}}^n}{3\Delta x}.$$

However, for the near boundary nodes $\delta_{2,x} E_{y_{\frac{1}{2}, j+\frac{1}{2}}}^n$ and $\delta_{2,x} E_{y_{I-\frac{1}{2}, j+\frac{1}{2}}}^n$ go out of domain. We can define

$$\begin{aligned} \tilde{\delta}_{2,x} E_{y_{\frac{1}{2}, j+\frac{1}{2}}}^n &= \frac{E_{y_{1, j+\frac{1}{2}}}^n + E_{y_{2, j+\frac{1}{2}}}^n - 2E_{y_{0, j+\frac{1}{2}}}^n}{3\Delta x}, \\ \tilde{\delta}_{2,x} E_{y_{I-\frac{1}{2}, j+\frac{1}{2}}}^n &= \frac{2E_{y_{I, j+\frac{1}{2}}}^n - E_{y_{I-1, j+\frac{1}{2}}}^n - E_{y_{I-2, j+\frac{1}{2}}}^n}{3\Delta x}, \end{aligned}$$

where the following relations [9] are used on the boundary nodes:

$$\begin{aligned} E_y(x_{-1}, y_{j+\frac{1}{2}}, t) &= 2E_y(x_0, y_{j+\frac{1}{2}}, t) - E_y(x_1, y_{j+\frac{1}{2}}, t) + O(\Delta x^5), \\ E_y(x_{I+1}, y_{j+\frac{1}{2}}, t) &= 2E_y(x_I, y_{j+\frac{1}{2}}, t) - E_y(x_{I-1}, y_{j+\frac{1}{2}}, t) + O(\Delta x^5). \end{aligned}$$

Thus, for the near boundary points with $i = 1$ and $i = I-1$,

$$\begin{aligned} \tilde{\Lambda}_x E_{y_{\frac{1}{2}, j+\frac{1}{2}}}^n &= \frac{1}{8}(9\delta_x - \tilde{\delta}_{2,x})E_{y_{\frac{1}{2}, j+\frac{1}{2}}}^n, \\ \tilde{\Lambda}_x E_{y_{I-\frac{1}{2}, j+\frac{1}{2}}}^n &= \frac{1}{8}(9\delta_x - \tilde{\delta}_{2,x})E_{y_{I-\frac{1}{2}, j+\frac{1}{2}}}^n, \end{aligned}$$

for $j = 0, 1, \dots, J-1$. Similarly, we can define $\Lambda_y F_{\alpha, \beta}^m$ in the y -direction as well.

We can split the Maxwell's equations in each time interval $[t^n, t^{n+1}]$ as following:

$$(4) \quad \frac{\partial E_x}{\partial t} = \frac{1}{\epsilon} \frac{\partial H_z}{\partial y}, \frac{1}{2} \frac{\partial H_z}{\partial t} = \frac{1}{\mu} \frac{\partial E_x}{\partial y},$$

$$(5) \quad \frac{\partial E_y}{\partial t} = -\frac{1}{\epsilon} \frac{\partial H_z}{\partial x}, \frac{1}{2} \frac{\partial H_z}{\partial t} = -\frac{1}{\mu} \frac{\partial E_y}{\partial x}.$$

2.2. The EO-4th-EC Scheme. We propose the Even-Odd cycled 4th-Order EC-S-FDTD scheme, shorten to EO-4th-EC. The proposed scheme is a combination of the EC-S-FDTD(1,4) and Even-Odd cycle technique.

Stage 1: The Odd time step.

At every odd time step, from $t^{(2k)}$ to $t^{(2k+1)}$, use $E_x^{(2k)}$, $E_y^{(2k)}$ and $H_z^{(2k)}$ to compute $E_x^{(2k+1)}$, $E_y^{(2k+1)}$ and $H_z^{(2k+1)}$ by the fourth-order spatial scheme.

Stage 1.1: First, compute $E_y^{(2k+1)}$ and intermediate variable H_z^ using $H_z^{(2k)}$ and $E_y^{(2k)}$, for $j = 0, 1, \dots, J-1$. For the interior points, $i = 2, 3, \dots, I-2$,*

$$(6) \quad \frac{E_{y_{i,j+\frac{1}{2}}}^{(2k+1)} - E_{y_{i,j+\frac{1}{2}}}^{(2k)}}{\Delta t} = -\frac{1}{2\epsilon} \Lambda_x \{ H_{z_{i,j+\frac{1}{2}}}^* + H_{z_{i,j+\frac{1}{2}}}^{(2k)} \},$$

$$(7) \quad \frac{H_{z_{i+\frac{1}{2},j+\frac{1}{2}}}^* - H_{z_{i+\frac{1}{2},j+\frac{1}{2}}}^{(2k)}}{\Delta t} = -\frac{1}{2\mu} \Lambda_x \{ E_{y_{i+\frac{1}{2},j+\frac{1}{2}}}^{(2k+1)} + E_{y_{i+\frac{1}{2},j+\frac{1}{2}}}^{(2k)} \}.$$

For boundary nodes, $i = 1$ and $i = I-1$,

$$(8) \quad \frac{E_{y_{i,j+\frac{1}{2}}}^{(2k+1)} - E_{y_{i,j+\frac{1}{2}}}^{(2k)}}{\Delta t} = -\frac{1}{2\epsilon} \widetilde{\Lambda}_x \{ H_{z_{i,j+\frac{1}{2}}}^* + H_{z_{i,j+\frac{1}{2}}}^{(2k)} \},$$

$$(9) \quad \frac{H_{z_{i+\frac{1}{2},j+\frac{1}{2}}}^* - H_{z_{i+\frac{1}{2},j+\frac{1}{2}}}^{(2k)}}{\Delta t} = -\frac{1}{2\mu} \widetilde{\Lambda}_x \{ E_{y_{i+\frac{1}{2},j+\frac{1}{2}}}^{(2k+1)} + E_{y_{i+\frac{1}{2},j+\frac{1}{2}}}^{(2k)} \}.$$

Stage 1.2: Then compute $E_x^{(2k+1)}$ and $H_z^{(2k+1)}$ using H_z^ and $E_x^{(2k)}$, for $i = 0, 1, \dots, I-1$. For interior nodes, $j = 2, 3, \dots, J-2$,*

$$(10) \quad \frac{E_{x_{i+\frac{1}{2},j}}^{(2k+1)} - E_{x_{i+\frac{1}{2},j}}^{(2k)}}{\Delta t} = \frac{1}{2\epsilon} \Lambda_y \{ H_{z_{i+\frac{1}{2},j}}^{(2k+1)} + H_{z_{i+\frac{1}{2},j}}^* \},$$

$$(11) \quad \frac{H_{z_{i+\frac{1}{2},j+\frac{1}{2}}}^{(2k+1)} - H_{z_{i+\frac{1}{2},j+\frac{1}{2}}}^*}{\Delta t} = \frac{1}{2\mu} \Lambda_y \{ E_{x_{i+\frac{1}{2},j+\frac{1}{2}}}^{(2k+1)} + E_{x_{i+\frac{1}{2},j+\frac{1}{2}}}^{(2k)} \}.$$

For boundary nodes, $j = 1$ and $j = J-1$,

$$(12) \quad \frac{E_{x_{i+\frac{1}{2},j}}^{(2k+1)} - E_{x_{i+\frac{1}{2},j}}^{(2k)}}{\Delta t} = \frac{1}{2\epsilon} \widetilde{\Lambda}_y \{ H_{z_{i+\frac{1}{2},j}}^{(2k+1)} + H_{z_{i+\frac{1}{2},j}}^* \},$$

$$(13) \quad \frac{H_{z_{i+\frac{1}{2},j+\frac{1}{2}}}^{(2k+1)} - H_{z_{i+\frac{1}{2},j+\frac{1}{2}}}^*}{\Delta t} = \frac{1}{2\mu} \widetilde{\Lambda}_y \{ E_{x_{i+\frac{1}{2},j+\frac{1}{2}}}^{(2k+1)} + E_{x_{i+\frac{1}{2},j+\frac{1}{2}}}^{(2k)} \}.$$

Stage 2. The Even time step.

At every even time step, from $t^{(2k+1)}$ to $t^{(2k+2)}$, use $E_x^{(2k+1)}$, $E_y^{(2k+1)}$ and $H_z^{(2k+1)}$ to compute $E_x^{(2k+2)}$, $E_y^{(2k+2)}$ and $H_z^{(2k+2)}$ by firstly fourth order difference y -direction scheme and secondly fourth order difference x -direction scheme.

*Stage 2.1: First compute $E_x^{(2k+2)}$ and intermediate variable H_z^{**} using $H_z^{(2k+1)}$*

and $E_x^{(2k+1)}$, $i = 0, 1, \dots, I - 1$. For interior nodes, $j = 2, 3, \dots, J - 2$,

$$(14) \quad \frac{E_{x_{i+\frac{1}{2},j}}^{(2k+2)} - E_{x_{i+\frac{1}{2},j}}^{(2k+1)}}{\Delta t} = \frac{1}{2\epsilon} \Lambda_y \{ H_{z_{i+\frac{1}{2},j}}^{**} + H_{z_{i+\frac{1}{2},j}}^{(2k+1)} \},$$

$$(15) \quad \frac{H_{z_{i+\frac{1}{2},j+\frac{1}{2}}}^{**} - H_{z_{i+\frac{1}{2},j+\frac{1}{2}}}^{(2k+1)}}{\Delta t} = \frac{1}{2\mu} \Lambda_y \{ E_{y_{i+\frac{1}{2},j+\frac{1}{2}}}^{(2k+2)} + E_{y_{i+\frac{1}{2},j+\frac{1}{2}}}^{(2k+1)} \}.$$

For boundary nodes, $j = 1$ and $J - 1$,

$$(16) \quad \frac{E_{x_{i+\frac{1}{2},j}}^{(2k+2)} - E_{x_{i+\frac{1}{2},j}}^{(2k+1)}}{\Delta t} = \frac{1}{2\epsilon} \widetilde{\Lambda}_y \{ H_{z_{i+\frac{1}{2},j}}^{**} + H_{z_{i+\frac{1}{2},j}}^{(2k+1)} \},$$

$$(17) \quad \frac{H_{z_{i+\frac{1}{2},j+\frac{1}{2}}}^{**} - H_{z_{i+\frac{1}{2},j+\frac{1}{2}}}^{(2k+1)}}{\Delta t} = \frac{1}{2\mu} \widetilde{\Lambda}_y \{ E_{y_{i+\frac{1}{2},j+\frac{1}{2}}}^{(2k+2)} + E_{y_{i+\frac{1}{2},j+\frac{1}{2}}}^{(2k+1)} \}.$$

Stage 2.2: Then compute $E_y^{(2k+2)}$ and $H_z^{(2k+2)}$ using H_z^{**} and $E_y^{(2k+1)}$, $j = 0, 1, \dots, J - 1$. For interior nodes, $i = 2, 3, \dots, I - 2$,

$$(18) \quad \frac{E_{y_{i,j+\frac{1}{2}}}^{(2k+2)} - E_{y_{i,j+\frac{1}{2}}}^{(2k+1)}}{\Delta t} = -\frac{1}{2\epsilon} \Lambda_x \{ H_{z_{i,j+\frac{1}{2}}}^{(2k+2)} + H_{z_{i,j+\frac{1}{2}}}^{**} \},$$

$$(19) \quad \frac{H_{z_{i+\frac{1}{2},j+\frac{1}{2}}}^{(2k+2)} - H_{z_{i+\frac{1}{2},j+\frac{1}{2}}}^{**}}{\Delta t} = -\frac{1}{2\mu} \Lambda_x \{ E_{y_{i+\frac{1}{2},j+\frac{1}{2}}}^{(2k+2)} + E_{y_{i+\frac{1}{2},j+\frac{1}{2}}}^{(2k+1)} \}.$$

For boundary nodes, $i = 1$, and $i = I - 1$,

$$(20) \quad \frac{E_{y_{i,j+\frac{1}{2}}}^{(2k+2)} - E_{y_{i,j+\frac{1}{2}}}^{(2k+1)}}{\Delta t} = -\frac{1}{2\epsilon} \widetilde{\Lambda}_x \{ H_{z_{i,j+\frac{1}{2}}}^{(2k+2)} + H_{z_{i,j+\frac{1}{2}}}^{**} \},$$

$$(21) \quad \frac{H_{z_{i+\frac{1}{2},j+\frac{1}{2}}}^{(2k+2)} - H_{z_{i+\frac{1}{2},j+\frac{1}{2}}}^{**}}{\Delta t} = -\frac{1}{2\mu} \widetilde{\Lambda}_x \{ E_{y_{i+\frac{1}{2},j+\frac{1}{2}}}^{(2k+2)} + E_{y_{i+\frac{1}{2},j+\frac{1}{2}}}^{(2k+1)} \}.$$

The boundary conditions are given by

$$E_{x_{i+\frac{1}{2},0}}^* = E_{x_{i+\frac{1}{2},J}}^* = E_{x_{i+\frac{1}{2},0}}^{(2k+2)} = E_{x_{i+\frac{1}{2},J}}^{(2k+2)} = E_{y_{0,j+\frac{1}{2}}}^{(2k+2)} = E_{y_{I,j+\frac{1}{2}}}^{(n+1)} = 0,$$

and the initial conditions are given by

$$\begin{aligned} E_{x_{\alpha,\beta}}^0 &= E_{x0}(\alpha\Delta x, \beta\Delta y), & E_{y_{\alpha,\beta}}^0 &= E_{y0}(\alpha\Delta x, \beta\Delta y), \\ H_{z_{\alpha,\beta}}^0 &= H_{z0}(\alpha\Delta x, \beta\Delta y). \end{aligned}$$

3. Dispersion Analysis

We take the dispersion analysis for our EO-4th-EC scheme. According to the Fourier Analysis, we define that for the time step $2k$ to $2k + 1$,

$$(22) \quad E_{\alpha,\beta}^{(2k+1)} = E^{(2k)} \xi^{(1)} e^{-i(k_x \alpha \Delta x + k_y \beta \Delta y)},$$

$$(23) \quad H_{\alpha,\beta}^{(2k+1)} = H_z^{(2k)} \xi^{(1)} e^{-i(k_x \alpha \Delta x + k_y \beta \Delta y)}.$$

And for time step $2k + 1$ to $2k + 2$, we let

$$(24) \quad E_{\alpha,\beta}^{(2k+2)} = E^{(2k+1)} \xi^{(2)} e^{-i(k_x \alpha \Delta x + k_y \beta \Delta y)},$$

$$(25) \quad H_{\alpha,\beta}^{(2k+2)} = H_z^{(2k+1)} \xi^{(2)} e^{-i(k_x \alpha \Delta x + k_y \beta \Delta y)}.$$

Here $\xi^{(1)}$ and $\xi^{(2)}$ are the growth factors for each time step. Growth factors are complex time eigenvalues whose magnitude will determine the stability and dissipation properties of the numerical scheme. $\mathbf{K}=(k_x, k_y)$ is the real wave number of the arbitrary harmonic wave component.

3.1. Equivalent Forms. Equivalent expressions are formed by eliminating the intermediate terms in the EO-4th-EC scheme and have them in a simplified form.

Equivalent Expression for the EO-4th-EC Scheme

For the odd time step, it gets

$$(26) \quad \frac{E_{x_{i+\frac{1}{2},j}}^{(2k+1)} - E_{x_{i+\frac{1}{2},j}}^{(2k)}}{\Delta t} = \frac{1}{2\epsilon} \Lambda_y \left\{ H_{z_{i+\frac{1}{2},j}}^{(2k+1)} + H_{z_{i+\frac{1}{2},j}}^{(2k)} \right\} - \frac{\Delta t}{4\mu\epsilon} \Lambda_x \Lambda_y \left\{ E_{y_{i+\frac{1}{2},j}}^{(2k+1)} + E_{y_{i+\frac{1}{2},j}}^{(2k)} \right\},$$

$$(27) \quad \frac{E_{y_{i,j+\frac{1}{2}}}^{(2k+1)} - E_{y_{i,j+\frac{1}{2}}}^{(2k)}}{\Delta t} = -\frac{1}{2\epsilon} \Lambda_x \left\{ H_{z_{i,j+\frac{1}{2}}}^{(2k+1)} + H_{z_{i,j+\frac{1}{2}}}^{(2k)} \right\} + \frac{\Delta t}{4\mu\epsilon} \Lambda_x \Lambda_y \left\{ E_{x_{i,j+\frac{1}{2}}}^{(2k+1)} + E_{x_{i,j+\frac{1}{2}}}^{(2k)} \right\},$$

$$(28) \quad \frac{H_{z_{i+\frac{1}{2},j+\frac{1}{2}}}^{(2k+1)} - H_{z_{i+\frac{1}{2},j+\frac{1}{2}}}^{(2k)}}{\Delta t} = \frac{1}{2\mu} \left\{ \Lambda_y \left\{ E_{x_{i+\frac{1}{2},j+\frac{1}{2}}}^{(2k+1)} + E_{x_{i+\frac{1}{2},j+\frac{1}{2}}}^{(2k)} \right\} - \Lambda_x \left\{ E_{y_{i+\frac{1}{2},j+\frac{1}{2}}}^{(2k+1)} + E_{y_{i+\frac{1}{2},j+\frac{1}{2}}}^{(2k)} \right\} \right\}.$$

For the even time step, it gets

$$(29) \quad \frac{E_{x_{i+\frac{1}{2},j}}^{(2k+2)} - E_{x_{i+\frac{1}{2},j}}^{(2k+1)}}{\Delta t} = \frac{1}{2\epsilon} \Lambda_y \left\{ H_{z_{i+\frac{1}{2},j}}^{(2k+2)} + H_{z_{i+\frac{1}{2},j}}^{(2k+1)} \right\} + \frac{\Delta t}{4\mu\epsilon} \Lambda_x \Lambda_y \left\{ E_{y_{i+\frac{1}{2},j}}^{(2k+2)} + E_{y_{i+\frac{1}{2},j}}^{(2k+1)} \right\},$$

$$(30) \quad \frac{E_{y_{i,j+\frac{1}{2}}}^{(2k+2)} - E_{y_{i,j+\frac{1}{2}}}^{(2k+1)}}{\Delta t} = -\frac{1}{2\epsilon} \Lambda_x \left\{ H_{z_{i,j+\frac{1}{2}}}^{(2k+2)} + H_{z_{i,j+\frac{1}{2}}}^{(2k+1)} \right\} - \frac{\Delta t}{4\mu\epsilon} \Lambda_x \Lambda_y \left\{ E_{x_{i,j+\frac{1}{2}}}^{(2k+2)} + E_{x_{i,j+\frac{1}{2}}}^{(2k+1)} \right\},$$

$$(31) \quad \frac{H_{z_{i+\frac{1}{2},j+\frac{1}{2}}}^{(2k+2)} - H_{z_{i+\frac{1}{2},j+\frac{1}{2}}}^{(2k+1)}}{\Delta t} = \frac{1}{2\mu} \left\{ \Lambda_y \left\{ E_{x_{i+\frac{1}{2},j+\frac{1}{2}}}^{(2k+2)} + E_{x_{i+\frac{1}{2},j+\frac{1}{2}}}^{(2k+1)} \right\} - \Lambda_x \left\{ E_{y_{i+\frac{1}{2},j+\frac{1}{2}}}^{(2k+2)} + E_{y_{i+\frac{1}{2},j+\frac{1}{2}}}^{(2k+1)} \right\} \right\}.$$

3.2. Stability Analysis for the EO-4th-EC Scheme. For the odd time step, we substitute equations (22)(23) into equivalent expressions (26)-(28) to analyze the stability for which we get the following system:

$$(32) \quad AX^{(2k)} = 0,$$

where $X^{(2k)} = [E_x^{(2k)}, E_y^{(2k)}, H_z^{(2k)}]^\tau$ and A is the coefficient matrix (33) for the odd time step with

$$(33) \quad A = \begin{bmatrix} \xi^{(1)} - 1 & -\frac{\Delta t^2}{\mu\epsilon} u_x v_y (\xi^{(1)} + 1) & -i\frac{\Delta t}{\epsilon} v_y (\xi^{(1)} + 1) \\ \frac{\Delta t^2}{\mu\epsilon} u_x v_y (\xi^{(1)} + 1) & (\xi^{(1)} - 1) & i\frac{\Delta t}{\epsilon} u_x (\xi^{(1)} + 1) \\ -i\frac{\Delta t}{\mu} v_y (\xi^{(1)} + 1) & i\frac{\Delta t}{\mu} u_x (\xi^{(1)} + 1) & (\xi^{(1)} - 1) \end{bmatrix},$$

$$u_x = \frac{\sin(\frac{3k_x \Delta x}{2}) - 27 \sin(\frac{k_x \Delta x}{2})}{24\Delta x}, v_y = \frac{\sin(\frac{3k_y \Delta y}{2}) - 27 \sin(\frac{k_y \Delta y}{2})}{24\Delta y}.$$

In order to find the growth matrix of the odd time step, we solve $\det(A) = 0$. The following equation is obtained

$$(34) \quad (\xi^{(1)} - 1)[Q\xi^{(1)2} + 2R\xi^{(1)} + Q] = 0,$$

where,

$$(35) \quad Q = 1 + \frac{\Delta t^2}{\mu\epsilon} (u_x^2 + v_y^2) + \frac{\Delta t^4}{\mu^2 \epsilon^2} u_x^2 v_y^2,$$

$$(36) \quad R = -1 + \frac{\Delta t^2}{\mu\epsilon} (u_x^2 + v_y^2) + \frac{\Delta t^4}{\mu^2 \epsilon^2} u_x^2 v_y^2.$$

The roots of (34) are $\xi_1^{(1)} = 1$ and $\xi_{2,3}^{(1)} = -\frac{R}{Q} \pm i\frac{\sqrt{Q^2 - R^2}}{Q}$ and we have $|\xi_{2,3}^{(1)}| = 1$.

For the even time step, similarly substituting equations (24)-(25) into equivalent expressions (29)-(31), we get

$$(37) \quad BX^{(2k+1)} = 0,$$

where $X^{(2k+1)} = [E_x^{(2k+1)}, E_y^{(2k+1)}, H_z^{(2k+1)}]^\tau$ and B is the coefficient matrix (38) for the even time step.

$$(38) \quad B = \begin{bmatrix} \xi^{(2)} - 1 & \frac{\Delta t^2}{\mu\epsilon} u_x v_y (\xi^{(2)} + 1) & -i\frac{\Delta t}{\epsilon} v_y (\xi^{(2)} + 1) \\ -\frac{\Delta t^2}{\mu\epsilon} u_x v_y (\xi^{(2)} + 1) & (\xi^{(2)} - 1) & i\frac{\Delta t}{\epsilon} u_x (\xi^{(2)} + 1) \\ -i\frac{\Delta t}{\mu} v_y (\xi^{(2)} + 1) & i\frac{\Delta t}{\mu} u_x (\xi^{(2)} + 1) & (\xi^{(2)} - 1) \end{bmatrix}.$$

Solving for $\det(B) = 0$, we get the following equation:

$$(39) \quad (\xi^{(2)} - 1)[Q\xi^{(2)2} + 2R\xi^{(2)} + Q] = 0.$$

Here the roots are $\xi_1^{(2)} = 1$, $\xi_{2,3}^{(2)} = -\frac{R}{Q} \pm i\frac{\sqrt{Q^2 - R^2}}{Q}$ and we have $|\xi_{2,3}^{(2)}| = 1$.

The growth factor for the scheme combining Stage 1 with Stage 2 is $\xi = \xi^{(1)}\xi^{(2)}$. By calculating, we have that

$$(40) \quad \xi = \begin{cases} \frac{2R^2 - Q^2}{Q^2} + i\frac{2R\sqrt{Q^2 - R^2}}{Q^2}, \\ 1, \\ \frac{2R^2 - Q^2}{Q^2} - i\frac{2R\sqrt{Q^2 - R^2}}{Q^2}. \end{cases}$$

It is clear that $|\xi| = 1$. Thus, we have the following theorem.

Theorem 1. *The EO-4th-EC Scheme is non-dissipative and unconditionally stable.*

3.3. Dispersion Relationship. The solution ξ of the characteristic polynomial equation of (34) and (39) determines the dispersion properties of the scheme. $|\xi|$ determines the amplitude (or dissipative) error, for which $\arctan(\text{Im}\xi/\text{Re}\xi)$ determines phase (or dispersive error) which is found in Section 5.

First, we can find the dispersion relationship for the EO-4th-EC scheme. We let $\gamma = j\omega$ and let

$$(41) \quad \xi^{(1)} = \xi^{(2)} = \xi_l = e^{\gamma\Delta t n}.$$

Since the growth factors for the odd and even time step are same, we get the same dispersion relationships for both even and odd time steps. To find the dispersion relationship for each time step, we consider the part with complex roots of the stability equations (34) and (39):

$$(42) \quad Q\xi_l^2 + 2R\xi_l + Q = 0.$$

By simplifying and dividing every term by $\xi^{(l)}$ and we get

$$(43) \quad Q(\xi_l + \xi_l^{-1}) + 2R = 0.$$

Using the definition (41), we get

$$(44) \quad \xi_l + \xi_l^{-1} = -4 \sin^2\left(\frac{\omega\Delta t}{2}\right) + 2.$$

Substituting equation (44), (35) and (36) into equation (43), we get

$$(45) \quad \begin{aligned} & \left[1 + \frac{\Delta t^2}{\mu\epsilon}(u_x^2 + v_y^2) + \frac{\Delta t^4}{\mu^2\epsilon^2}u_x^2v_y^2\right](-4 \sin^2\left(\frac{\omega\Delta t}{2}\right) + 2) \\ & + 2\left[-1 + \frac{\Delta t^2}{\mu\epsilon}(u_x^2 + v_y^2) + \frac{\Delta t^4}{\mu^2\epsilon^2}u_x^2v_y^2\right] = 0. \end{aligned}$$

Simplifying we get the dispersion relationship

$$(46) \quad \left[\frac{\Delta t^2}{\mu\epsilon}(u_x^2 + v_y^2) + \frac{\Delta t^4}{\mu^2\epsilon^2}u_x^2v_y^2\right] \cos^2\left(\frac{\omega\Delta t}{2}\right) = \sin^2\left(\frac{\omega\Delta t}{2}\right).$$

Using the definition of u_x and v_y ,

$$\begin{aligned} & \left\{ \frac{\Delta t^2}{\mu\epsilon} \left\{ \left(\frac{\sin\left(\frac{3k_x\Delta x}{2}\right) - 27 \sin\left(\frac{k_x\Delta x}{2}\right)}{24\Delta x} \right)^2 + \left(\frac{\sin\left(\frac{3k_y\Delta y}{2}\right) - 27 \sin\left(\frac{k_y\Delta y}{2}\right)}{24\Delta y} \right)^2 \right\} \right. \\ & \left. + \frac{\Delta t^4}{\mu^2\epsilon^2} \left(\frac{\sin\left(\frac{3k_x\Delta x}{2}\right) - 27 \sin\left(\frac{k_x\Delta x}{2}\right)}{24\Delta x} \right)^2 \left(\frac{\sin\left(\frac{3k_y\Delta y}{2}\right) - 27 \sin\left(\frac{k_y\Delta y}{2}\right)}{24\Delta y} \right)^2 \right\} \cos^2\left(\frac{\omega\Delta t}{2}\right) \\ & = \sin^2\left(\frac{\omega\Delta t}{2}\right), \end{aligned}$$

which can be simplified to the dispersion relationship for the EO-4th-EC Scheme as

$$(47) \quad \begin{aligned} & \left\{ \Delta t^2 c^2 \left\{ \left(\frac{\sin\left(\frac{3k_x\Delta x}{2}\right) - 27 \sin\left(\frac{k_x\Delta x}{2}\right)}{24\Delta x} \right)^2 + \left(\frac{\sin\left(\frac{3k_y\Delta y}{2}\right) - 27 \sin\left(\frac{k_y\Delta y}{2}\right)}{24\Delta y} \right)^2 \right\} + \right. \\ & \left. \Delta t^4 c^4 \left(\frac{\sin\left(\frac{3k_x\Delta x}{2}\right) - 27 \sin\left(\frac{k_x\Delta x}{2}\right)}{24\Delta x} \right)^2 \left(\frac{\sin\left(\frac{3k_y\Delta y}{2}\right) - 27 \sin\left(\frac{k_y\Delta y}{2}\right)}{24\Delta y} \right)^2 \right\} \cos^2\left(\frac{\omega\Delta t}{2}\right) \\ & = \sin^2\left(\frac{\omega\Delta t}{2}\right), \end{aligned}$$

where $c = \frac{1}{\sqrt{\mu\epsilon}}$. Note, here $k_x = k \cos(\phi)$ and $k_y = k \sin(\phi)$. As $\Delta t, \Delta x, \Delta y \rightarrow 0$, the dispersion relationship converges to

$$k_x^2 + k_y^2 = \frac{\omega^2}{c^2}.$$

4. Energy Conservation

For grid functions defined on the staggered grid $U := \{U_{i+\frac{1}{2},j}\}$, $V := \{V_{i,j+\frac{1}{2}}\}$, $W = \{W_{i+\frac{1}{2},j+\frac{1}{2}}\}$, $\vec{F} := \{(U_{i+\frac{1}{2},j}, V_{i,j+\frac{1}{2}})\}$, the discrete L^2 energy norms are used as

$$\begin{aligned} \|U\|_{E_x}^2 &= \sum_{i=0}^{I-1} \sum_{j=0}^{J-1} |U_{i+\frac{1}{2},j}|^2 \Delta x \Delta y, \quad \|V\|_{E_y}^2 = \sum_{i=0}^{I-1} \sum_{j=0}^{J-1} |V_{i,j+\frac{1}{2}}|^2 \Delta x \Delta y, \\ \|W\|_H^2 &= \sum_{i=0}^{I-1} \sum_{j=0}^{J-1} |W_{i+\frac{1}{2},j+\frac{1}{2}}|^2 \Delta x \Delta y, \quad \|\vec{F}\|_E^2 = \|U\|_{E_x}^2 + \|V\|_{E_y}^2. \end{aligned}$$

Theorem 2 (Discrete Energy Conservations). *For integer $n \geq 0$, if $\vec{E}^n := \{(E_{x_{i+\frac{1}{2},j}}^n, E_{y_{i,j+\frac{1}{2}}}^n)\}$ and $H_z^n := \{H_{z_{i+\frac{1}{2},j+\frac{1}{2}}}^n\}$ are the solutions of EO-4th-EC scheme, then the following discrete energies are constant.*

$$(48) \quad \|\epsilon^{\frac{1}{2}} \vec{E}^{n+1}\|_E^2 + \|\mu^{\frac{1}{2}} H_z^{n+1}\|_H^2 = \|\epsilon^{\frac{1}{2}} \vec{E}^n\|_E^2 + \|\mu^{\frac{1}{2}} H_z^n\|_H^2,$$

where $n = 2k$ and $2k + 1$, and

$$\begin{aligned} (49) \quad \|\epsilon^{\frac{1}{2}} \frac{(\vec{E}^{n+2} - \vec{E}^n)}{(2\Delta t)}\|_E^2 + \|\mu^{\frac{1}{2}} \frac{(H_z^{n+2} - H_z^n)}{(2\Delta t)}\|_H^2 \\ = \|\epsilon^{\frac{1}{2}} \frac{(\vec{E}^{n+1} - \vec{E}^{n-1})}{(2\Delta t)}\|_E^2 + \|\mu^{\frac{1}{2}} \frac{(H_z^{n+1} - H_z^{n-1})}{(2\Delta t)}\|_H^2, \end{aligned}$$

where $n = 2k$ and $2k + 1$.

Proof. Multiplying both sides of (6) with $\epsilon\Delta t(E_{i,j+\frac{1}{2}}^{2k+1} + E_{i,j+\frac{1}{2}}^{2k})$ and Multiplying both sides of (7) with $\mu\Delta t(H_{i+\frac{1}{2},j+\frac{1}{2}}^* + H_{i+\frac{1}{2},j+\frac{1}{2}}^{2k})$, we can get

$$\begin{aligned} (50) \quad \epsilon \left[(E_{y_{i,j+\frac{1}{2}}}^{(2k+1)})^2 - (E_{y_{i,j+\frac{1}{2}}}^{(2k)})^2 \right] \\ = -\frac{\Delta t}{2} A_x (H_{z_{i+\frac{1}{2},j+\frac{1}{2}}}^* + H_{z_{i+\frac{1}{2},j+\frac{1}{2}}}^{(2k)}) (E_{y_{i,j+\frac{1}{2}}}^{(2k+1)} + E_{y_{i,j+\frac{1}{2}}}^{(2k)}), \end{aligned}$$

$$\begin{aligned} (51) \quad \mu \left[(H_{z_{i+\frac{1}{2},j+\frac{1}{2}}}^*)^2 - (H_{z_{i+\frac{1}{2},j+\frac{1}{2}}}^{(2k)})^2 \right] \\ = -\frac{\Delta t}{2} A_x (E_{y_{i+\frac{1}{2},j+\frac{1}{2}}}^{(2k+1)} + E_{y_{i+\frac{1}{2},j+\frac{1}{2}}}^{(2k)}) (H_{z_{i+\frac{1}{2},j+\frac{1}{2}}}^* + H_{z_{i+\frac{1}{2},j+\frac{1}{2}}}^{(2k)}). \end{aligned}$$

Sum over all the terms in the above two equations, and add them together. Note that E_y satisfies the boundary condition $(E, 0) \times (\mathbf{n}, 0) = 0$ on $(0, T] \times \partial\Omega$, where \mathbf{n} is the outward normal vector on $\partial\Omega$, then by Lemma 9 in [1] we have

$$\begin{aligned} (52) \quad \sum_{i=0}^{I-1} \sum_{j=0}^{J-1} (\epsilon (E_{y_{i,j+\frac{1}{2}}}^{(2k+1)})^2 + \mu (H_{z_{i+\frac{1}{2},j+\frac{1}{2}}}^*)^2) \\ = \sum_{i=0}^{I-1} \sum_{j=0}^{J-1} (\epsilon (E_{y_{i,j+\frac{1}{2}}}^{(2k)})^2 + \mu (H_{z_{i+\frac{1}{2},j+\frac{1}{2}}}^{(2k)})^2). \end{aligned}$$

Similarly, from (10)(11), we have

$$(53) \quad \sum_{i=0}^{I-1} \sum_{j=0}^{J-1} (\epsilon(E_{x_{i+\frac{1}{2},j}}^{(2k+1)})^2 + \mu(H_{z_{i+\frac{1}{2},j+\frac{1}{2}}}^*)^2) \\ = \sum_{i=0}^{I-1} \sum_{j=0}^{J-1} (\epsilon(E_{x_{i+\frac{1}{2},j}}^{(2k)})^2 + \mu(H_{z_{i+\frac{1}{2},j+\frac{1}{2}}}^*)^2).$$

Similarly, the same can be done for the even time step. Equations (51) and (52) get (48). Let us consider one time period ($n = 2k$), we use (14)(15) and (18)(19). Subtracting the $(2k)$ th step from $(2k+2)$ th step of the EO-4th-EC scheme, we get

$$(54) \quad \frac{E_{x_{i+\frac{1}{2},j}}^{(2k+2)} - E_{x_{i+\frac{1}{2},j}}^{(2k)}}{\Delta t} - \frac{E_{x_{i+\frac{1}{2},j}}^{(2k+1)} - E_{x_{i+\frac{1}{2},j}}^{(2k-1)}}{\Delta t} \\ = \frac{1}{2\epsilon} A_y \{ (H_{z_{i+\frac{1}{2},j}}^{**} - H_{z_{i+\frac{1}{2},j}}^{** - 2}) + (H_{z_{i+\frac{1}{2},j}}^{(2k+1)} - H_{z_{i+\frac{1}{2},j}}^{(2k-1)}) \},$$

$$(55) \quad \frac{H_{z_{i+\frac{1}{2},j+\frac{1}{2}}}^{**} - H_{z_{i+\frac{1}{2},j+\frac{1}{2}}}^{** - 2}}{\Delta t} - \frac{H_{z_{i+\frac{1}{2},j+\frac{1}{2}}}^{2k+1} - H_{z_{i+\frac{1}{2},j+\frac{1}{2}}}^{(2k-1)}}{\Delta t} \\ = \frac{1}{2\mu} A_y \{ (E_{x_{i+\frac{1}{2},j+\frac{1}{2}}}^{(2k+2)} - E_{x_{i+\frac{1}{2},j+\frac{1}{2}}}^{(2k)}) + (E_{x_{i+\frac{1}{2},j+\frac{1}{2}}}^{(2k+1)} - E_{x_{i+\frac{1}{2},j+\frac{1}{2}}}^{(2k-1)}) \},$$

$$(56) \quad \frac{E_{y_{i,j+\frac{1}{2}}}^{(2k+2)} - E_{y_{i,j+\frac{1}{2}}}^{(2k)}}{\Delta t} - \frac{E_{y_{i,j+\frac{1}{2}}}^{(2k+1)} - E_{y_{i,j+\frac{1}{2}}}^{(2k-1)}}{\Delta t} \\ = -\frac{1}{2\epsilon} A_x \{ (H_{z_{i,j+\frac{1}{2}}}^{(2k+2)} - H_{z_{i,j+\frac{1}{2}}}^{(2k)}) + (H_{z_{i,j+\frac{1}{2}}}^{**} - H_{z_{i,j+\frac{1}{2}}}^{** - 2}) \},$$

$$(57) \quad \frac{H_{z_{i+\frac{1}{2},j+\frac{1}{2}}}^{(2k+2)} - H_{z_{i+\frac{1}{2},j+\frac{1}{2}}}^{(2k)}}{\Delta t} - \frac{H_{z_{i+\frac{1}{2},j+\frac{1}{2}}}^{**} - H_{z_{i+\frac{1}{2},j+\frac{1}{2}}}^{** - 2}}{\Delta t} \\ = \frac{1}{2\mu} A_x \{ (E_{y_{i+\frac{1}{2},j+\frac{1}{2}}}^{(2k+2)} - E_{y_{i+\frac{1}{2},j+\frac{1}{2}}}^{(2k)}) + (E_{y_{i+\frac{1}{2},j+\frac{1}{2}}}^{(2k+1)} - E_{y_{i+\frac{1}{2},j+\frac{1}{2}}}^{(2k-1)}) \}.$$

Note that $\frac{E^{(2k+2)} - E^{(2k)}}{2\Delta t}$ also satisfies the boundary condition, then following the proof of discrete energy conservation I and using Lemma 9 in paper [1], we can get the second discrete energy conservation. \square

Theorem 2 shows that the EO-4th-EC scheme satisfies the Poynting theorem in discrete sense and the energy conservation in discrete time variation holds at every two time steps.

5. Numerical Tests

5.1. Phase Error. We can now present the numerical dispersion errors of the proposed scheme compared to other schemes with different wave propagation angles, different grid sizes and CFL numbers.

Let $\xi = e^{(i\omega 2\Delta t)}$, where ω is a complex number: $\omega = \omega_R$ and ω_I are the real and imaginary parts respectively. Then,

$$(58) \quad \xi = e^{-\omega_I 2\Delta t} (\cos(\omega_R 2\Delta t) + i \sin(\omega_R 2\Delta t)).$$

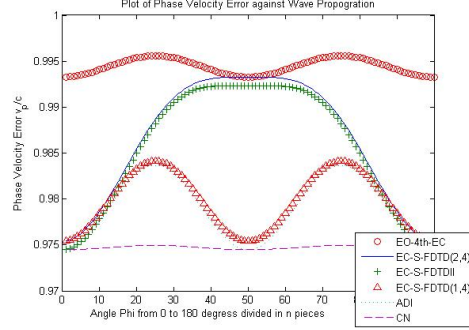


FIGURE 1. Numerical dispersion against the wave propagation angle phi from 0 to 180 degrees with $N_\lambda = 40$ and $S = 3.5$.

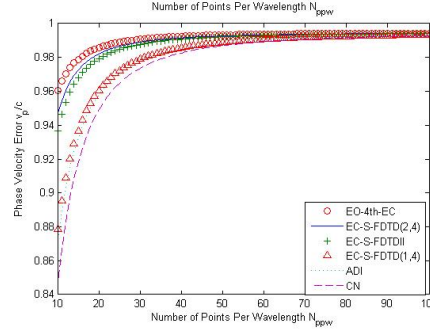


FIGURE 2. Numerical dispersion against number of points per wavelength, N_λ with $S = 3.5$, $\phi = 65$ degrees.

Let $Im(\xi)$ and $Re(\xi)$ be the imaginary and real parts of the growth factor ξ . The numerical phase velocity v_p is normalized to the speed of the wave c , also called phase velocity error as

$$(59) \quad \frac{v_p}{c} = \frac{N_\lambda}{2\pi S} \arctan\left(\frac{|Im(\xi)|}{|Re(\xi)|}\right),$$

where wavenumber $\mathbf{k} = (k_x, k_y)$ where $k_x = k \cos \phi$, $k_y = k \sin \phi$, and $\omega = ck$, $c = \frac{1}{\sqrt{\mu\epsilon}}$, $\lambda =$ wavelength, $\Delta x = \Delta y = h$ are the spatial step size, $N_\lambda = \frac{\lambda}{h} =$ number of points per wavelength (NPPW), $S = \frac{c\Delta t}{h} =$ CFL (Courant) number. For our even-odd energy conserved scheme, the above equation is used for which the real and imaginary parts of the stability factors are used.

Figure 1 shows the numerical phase error against wave propagation angle, ϕ , as it varies from 0° to 180° using parameters $N_\lambda = 40$ and $S = 3.5$. Figure 2 compares the numerical phase error against number of points per wavelength as they vary from 10 to 100 with parameters N_λ with $S = 3.5$, $\phi = 65^\circ$. Figure 3 compares the phase error against Courant number, CFL, with parameters $N_\lambda = 40$ and $\phi = 65^\circ$, where CFL number varies from 1 to 5. All three figures compare the proposed scheme with Crank Nicolson (CN), EC-S-FDTDII [1], ADI-FDTD [13,19], EC-S-FDTD(1,4) and EC-S-FDTD(2,4) [9] schemes. As shown in Figures 1, 2 and 3, the CN scheme has the worst phase velocity error comparing to other schemes. ADI-FDTD and EC-S-FDTDII schemes are although better than the CN

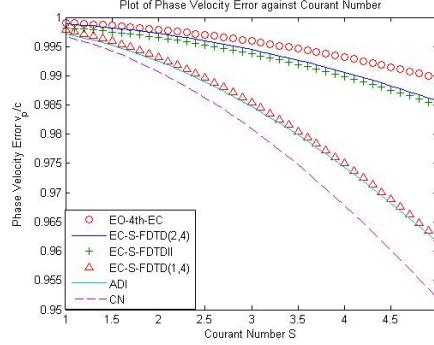


FIGURE 3. Numerical dispersion against CFL number with $N_\lambda = 40$ and $\phi = 65$ degrees.

TABLE 1. Relative Errors of Energies I and II of different schemes. Parameters: $T = 1$, $\Delta t = \Delta x = \Delta y = T/100$, $k_x = k_y = k$.

k	EC(1,4)		EC(2,4)		EO-4th-EC		ADI-FDTD	
	REE-I	REE-II	REE-I	REE-II	REE-I	REE-II	REE-I	REE-II
1	2.02e-14	1.76e-14	1.39e-14	1.26e-14	1.98e-14	1.78e-14	6.17e-5	2.88e-4
3	1.98e-14	1.86e-14	1.39e-14	1.27e-14	1.98e-14	1.81e-14	5.53e-4	2.61e-3
7	1.93e-14	1.94e-14	1.42e-14	1.42e-14	1.93e-14	1.94e-14	3.0e-3	1.39e-2

TABLE 2. Relative Error I in time step of numerical solutions of difference schemes, Parameters: $T = 1$, $k_x = k_y = 1$, $\mu = \epsilon = 1$, $\Delta t = \Delta x = \Delta y = 1/N$.

N	EC(1,4)		EC(2,4)		EO-4th-EC		ADI-FDTD	
	Error I	Ratio	Error I	Ratio	Error I	Ratio	Error I	Ratio
25	0.0434	–	0.0051	–	0.0126	–	0.0108	–
50	0.0215	1.013	0.0013	1.985	0.0032	1.977	0.0027	2.000
100	0.0107	1.007	3.2209e-4	1.999	7.9476e-4	2.009	6.7599e-4	1.998
200	0.0054	0.987	8.0527e-5	1.999	1.9870e-4	1.999	1.6902e-4	1.999

scheme, they are not as great as the EC-S-FDTD(2,4) or EC-S-FDTD(1,4) scheme. Comparing to all the other schemes, our scheme has the ratio v_p/c closest to 1. Also, Figure 3 shows that as CFL number increases, the phase error increases, whereas in Figure 2, as the number of points per wavelength increases, the phase velocity error decreases. Therefore, the numerical dispersion error of our scheme, EO-4th-EC scheme has the smallest error comparing to the other schemes.

5.2. Accuracy, Energy Conservation and Divergence Free Approximation. Now, we study numerically energy conservation, accuracy and convergence of divergence free of our scheme by comparing with other schemes. We consider the Maxwell's equations (1)-(3) in a lossless medium with the domain surrounded by a perfect conductor. The exact solution to Eqs. (1)-(3) is

$$(60) \quad E_x = \frac{k_y}{\epsilon\sqrt{\mu}\omega} \cos(\omega\pi t) \cos(k_x\pi x) \sin(k_y\pi y),$$

TABLE 3. Relative Error II in time step of numerical solutions of difference schemes. Parameters: $T = 1$, $k_x = k_y = 1$, $\mu = \epsilon = 1$, $\Delta t = \Delta x = \Delta y = 1/N$.

N	EC(1,4)		EC(2,4)		EO-4th-EC		ADI-FDTD	
	Error II	Ratio	Error II	Ratio	Error II	Ratio	Error II	Ratio
25	0.0173	–	0.0051	–	0.0114	–	0.0101	–
50	0.0071	1.285	0.0013	1.972	0.0031	1.879	0.0026	1.958
100	0.0032	1.149	3.2745e-4	1.989	7.7781e-4	1.995	6.4756e-4	2.005
200	0.0015	1.093	8.2070e-5	1.996	1.9550e-4	1.992	1.6246e-4	1.995

TABLE 4. Relative Error I in spatial step of numerical solutions of difference schemes. Parameters: $T = 1$, $k_x = k_y = 1$, $\mu = \epsilon = 1$, $\Delta t = \frac{1}{N^4}$ for EC(1,4) and $\Delta t = \frac{1}{N^2}$ for EC(2,4), ADI-FDTD and EO-4th-EC Schemes.

N	EC(1,4)		EC(2,4)		EO-4th-EC		ADI-FDTD	
	Error I	Ratio	Error I	Ratio	Error I	Ratio	Error I	Ratio
10	2.2837e-4	–	5.2279e-4	–	9.8328e-4	–	0.0187	–
15	4.5219e-5	3.994	1.0341e-4	3.997	1.9390e-4	4.004	0.0082	2.033
20	1.4320e-5	3.997	3.2735e-5	3.998	6.1518e-5	3.991	0.0046	2.009
25	5.8679e-6	3.998	1.3411e-5	3.999	2.5178e-5	4.004	0.0029	2.067
30	2.8305e-6	3.999	6.4682e-6	3.999	1.2154e-5	3.995	0.0020	2.038

TABLE 5. Relative Error II in spatial step of numerical solutions of difference schemes. Parameters: $T = 1$, $k_x = k_y = 1$, $\mu = \epsilon = 1$, $\Delta t = \frac{1}{N^4}$ for EC(1,4) and $\Delta t = \frac{1}{N^2}$ for EC(2,4), ADI-FDTD and EO-4th-EC Schemes.

N	EC(1,4)		EC(2,4)		EO-4th-EC		ADI-FDTD	
	Error II	Ratio	Error II	Ratio	Error II	Ratio	Error II	Ratio
10	2.0886e-4	–	5.3257e-4	–	9.7475e-4	–	0.0190	–
15	4.1383e-5	3.994	1.0564e-4	3.989	1.9298e-4	3.994	0.0084	2.013
20	1.3108e-5	3.997	3.3472e-5	3.995	6.1464e-5	3.977	0.0047	2.018
25	5.3719e-6	3.998	1.3719e-5	3.997	2.5162e-5	4.002	0.0030	2.012
30	2.5914e-6	3.999	6.6182e-6	3.998	1.2160e-5	3.989	0.0021	1.956

TABLE 6. Error of divergence free of divergence 1 in time step of numerical solutions of different schemes. Parameters: $T=1$, $k_x = k_y = 1$, $\mu = \epsilon = 1$, $\Delta t = \Delta x = \Delta y = \frac{1}{N}$.

N	EC(1,4)		EC(2,4)		EO-4th-EC		ADI-FDTD	
	Div 1	Ratio	Div 1	Ratio	Div 1	Ratio	Div 1	Ratio
25	0.1964	–	0.0044	–	0.0349	–	0.0174	–
50	0.0986	0.994	0.0011	2.000	0.0088	1.988	0.0044	1.984
100	0.0493	0.949	2.7404e-4	1.999	0.0022	2.000	0.0019	2.071
200	0.0247	0.997	6.8513e-5	1.999	5.4810e-4	2.005	0.0011	1.899

TABLE 7. Error of divergence free of divergence 2 in time step of numerical solutions of different schemes. Parameters: $T = 1$, $k_x = k_y = 1$, $\mu = \epsilon = 1$, $\Delta t = \Delta x = \Delta y = \frac{1}{N}$.

N	EC(1,4)		EC(2,4)		EO-4th-EC		ADI-FDTD	
	Div 2	Ratio	Div 2	Ratio	Div 2	Ratio	Div 2	Ratio
25	0.0982	–	0.0022	–	0.0175	–	0.0087	–
50	0.0493	0.994	5.4791e-4	2.005	0.0044	1.992	0.0022	1.984
100	0.0247	0.997	1.3702e-4	1.999	0.0011	2.000	9.7365e-4	2.010
200	0.0123	1.006	3.4256e-5	2.000	2.7405e-4	2.005	5.4798e-4	1.998

$$(61) \quad E_y = -\frac{k_x}{\epsilon\sqrt{\mu\omega}} \cos(\omega\pi t) \sin(k_x\pi x) \cos(k_y\pi y),$$

$$(62) \quad H_z = -\frac{1}{\sqrt{\mu}} \sin(\omega\pi t) \cos(k_x\pi x) \cos(k_y\pi y).$$

As shown in Table 1, ADI-FDTD is not energy-conserved. It has large errors of energy of $10^{-3} - 10^{-5}$ when compared to the other schemes EC(1,4), EC(2,4) and EO-4th-EC. Table 1 uses the parameters $\Delta t = \Delta x = \Delta y = 0.01$ and $k_x = k_y$. As the wavenumber \mathbf{k} increases, the errors of energy of EC(1,4), EC(2,4) and EO-4th-EC reaches 10^{-14} , which is mechanical error. Hence, these three schemes are energy-conserved.

Tables 2 and 3 compare relative accuracy of numerical solutions in time step for the four schemes using parameters, $T = 1$, $\Delta t = \Delta x = \Delta y = 1/N$, $\mu = \epsilon = 1$, $k_x = k_y = 1$. It is easily seen that EC(1,4) scheme is only first order in time step, where EC(1,4), ADI-FDTD and EO-4th-EC are all second order in time step. Comparing with the EC(2,4) scheme, our EO-4th-EC scheme takes much less time to run as it only requires two stages at each time step while EC(2,4) uses three stages at each time step.

Tables 4 and 5 compare the relative accuracy in spatial steps for four schemes with parameters, $T = 1$, $\Delta x = \Delta y = 1/N$, $\mu = \epsilon = 1$, $k_x = k_y = 1$, $\Delta t = 1/N^4$ for EC(1,4) and $\Delta t = 1/N^2$ for the other three schemes. The convergent ratio clearly states that ADI-FDTD scheme is second order in space where our scheme EO-4th-EC, and EC(1,4), EC(2,4) schemes are fourth-order accurate in space. Tables 2, 3, 4, and 5 prove that the proposed EO-4th-EC scheme is second order in time and fourth order in space.

Tables 6 and 7 list the numerical results of divergence free, Div1 and Div2, for the four schemes mentioned above with $\Delta t = \Delta x = \Delta y$ at time $t = 1$. It can be clearly seen that our EO-4th-EC, EC(2,4), ADI-FDTD schemes are all second order in time while EC(1,4) is first order in time.

6. Numerical Experiments

6.1. Wave Propagating Through Vacuum Domain With a Perfectly Matched Layer. First we consider a vacuum domain with an initial magnetic field as shown in Figure 4. The domain has symmetry about the z -axis and it makes the $\frac{\partial}{\partial z}$ components of the 3D Maxwell's equations equals to zero. We consider initial magnetic field in the z -direction, hence we use the TE model with E_x , E_y and H_z . We consider the Perfectly Matched Layer (PML) condition at the boundary.

In this experiment, we consider an initial magnetic field in the z -direction, H_{z0} . The initial magnetic field is positioned at the center of the domain. The boundary

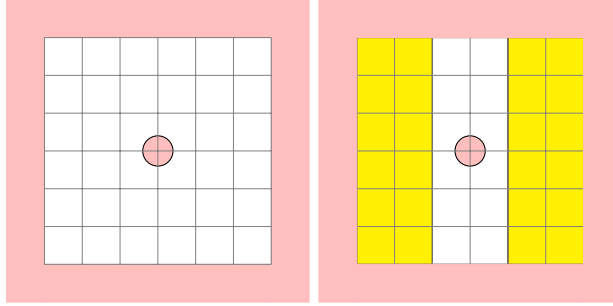


FIGURE 4. 2D Domains for a vacuum space (left) with Perfectly Matched Layer and for different materials (right) with Perfectly Matched layer.

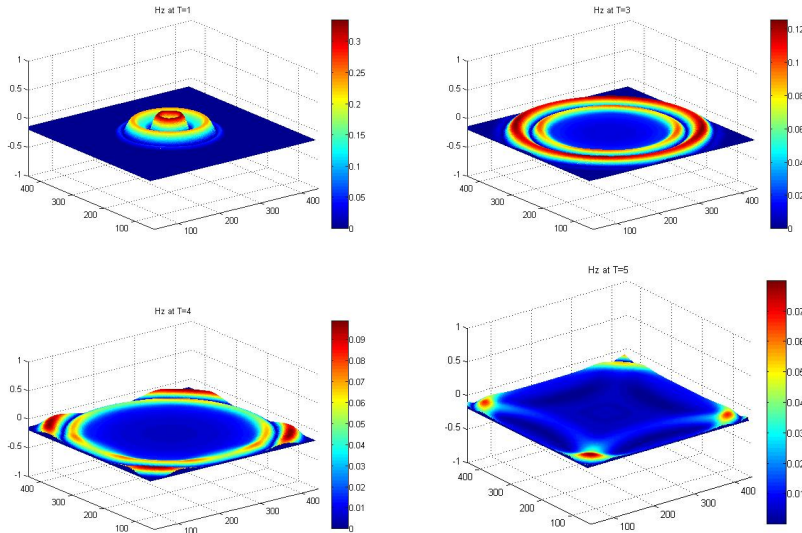


FIGURE 5. H_z with Initial Magnetic Field, Top: Left ($T = 1$), Right ($T = 3$), Bottom: Left ($T = 4$), Right ($T = 5$).

condition is $E_{x0} = 0, E_{y0} = 0$ and H_{z0} . The initial condition is

$$(63) \quad H_{z0} = \begin{cases} \frac{1}{25}(10 + 15 \sin(\frac{10}{3}\pi r)), & r < 0.5, \\ 0, & \text{otherwise.} \end{cases}$$

Figure 5 shows the magnetic field in z -direction in a case where initial magnetic field, H_{z0} , is present. As seen in this figure, the magnetic wave starts to travel outwards with increase in time. As the wave hits the perfectly matched layer, the wave smoothly makes an exit by being absorbed into the layer and creating no reflection.

6.2. Wave Propagating in Different Mediums With a Perfectly Matched Layer. This section focuses on wave propagation inside different mediums whose domain is surrounded by a Perfectly Matched Layer. The EO-4th-EC scheme is simulated in MATLAB. Symmetry in the z -axis is considered and hence, TE mode with E_x, E_y and H_z is used. In this case, we only consider the presence of an initial

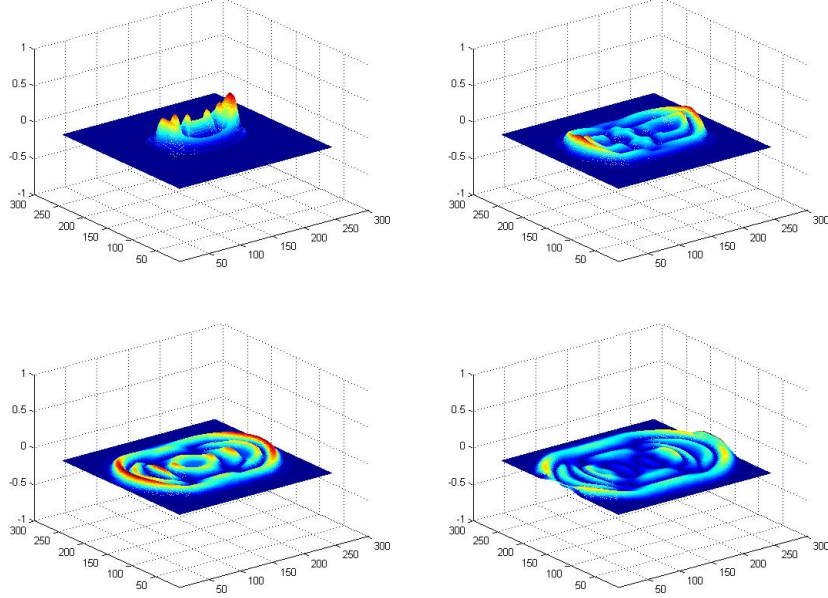


FIGURE 6. H_z with initial magnetic field, J_z in z -direction Vacuum (center) to Gold (left and right). Top: Left ($T = 1$), Right ($T = 3$), Bottom: Left ($T = 4$), Right ($T = 5$).

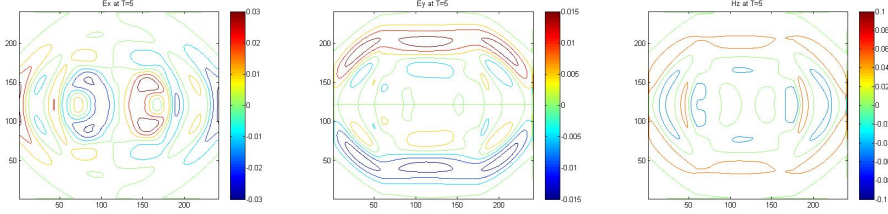


FIGURE 7. Contour for E_x , E_y and H_z at $T = 5$.

magnetic field in the z -direction. Figure 4 (right) shows the cross-section of the $x - y$ plane with the presence of a Perfectly matched layer. Initial magnetic field is defined as equation (63).

At the interface, electric permittivity and magnetic permeability is defined as follows. Relative Electric permittivity ϵ is

$$(64) \quad \epsilon = \begin{cases} 1, & a_1 < x < i_1, \\ 12, & i_1 < x < i_2, \\ 1, & i_2 < x < b_1. \end{cases}$$

and by paper [4], at the interface, ϵ is defined as

$$(65) \quad \epsilon = \begin{cases} \frac{1+12}{2}, & x = i_1, \\ \frac{1+12}{2}, & x = i_2. \end{cases}$$

Here, i_1 and i_2 are interfaces in Figure 6. μ can be defined similarly at the interface.

Figure 6 shows the magnetic field in z direction as the initial magnetic field travels through the domain. Bigger fraction of the magnetic field moves to the gold plate rather than traveling in the vacuum domain due to its higher electric permittivity. As it hits the boundary, the wave is absorbed into the domain making a smooth exit. Figure 7 shows the contour figures of E_x , E_y and H_z at $T = 5$. It can be easily seen that the wave changes as it moves to a different domain. This figure also shows the smooth exit each wave makes as it reaches the boundary.

6.3. Grounded Coplanar Waveguide with Current Due to Lumped Ports.

Grounded coplanar waveguide (GCPW) is made of dielectric substrate underneath the coplanar waveguide. It ensures that the electricity produced in the system does not interfere with other components of a printed circuit board. One of common materials used for a substrate is gallium arsenide, GaAs, with a electric permittivity of 12.9. Waveguide is a structure which guides electromagnetic waves. Most common waveguides contain metal pipe/line used to carry high frequencies, radio waves particularly microwaves. Metallic lines are used at microwave frequencies utilized to connect receivers and transmitters with antennas. The walls of a waveguide are made of conducting material not to conduct energy but for reflection of waves. Transmission lines are commonly used with sampling circuits for millimeter-wave instruments. CPWs are used in integrated circuits. Integrated circuits are used in all electronic equipment such as computers, mobile phones and other digital home appliances. CPWs are considered for use for millimeter-wave integrated circuits(MMIC) instead of microstrip. MMIC is an integrated circuit that operates at microwave frequencies of 300MHz to 300GHz. Inputs and Outputs are matched to Characteristic Impedance (Z) = 50 Ohms in a microwave frequency range. Coplanar waveguides are fabricated using semiconductor, Gallium Arsenide(GaAS). Other materials used are Si (Silicon), InP (Indium Phosphide), SiGe (Silicon Germanium), and GaN (Gallium Nitride). Depending on the output required, different fabrication is used. GaAs is the most common dielectric substrate for most transmission lines.

There are different ways to excite a GCPW. Adding a rectangular faces to the model, either normal or parallel to the plane of the CPW, along with a lumped port is one of the way to excite a CPW. A lumped port excitation is applied between the rectangular face and the center conductor. The arrows apply to show the direction of the flow of applied current that behaves sinusoidally dependent of time. Another simpler method is to include two lumped ports which either both travel towards or away from the center conductor. In this scenario, the structure is simpler, however two lumped ports are required to be manually set. A lumped port is a transmission connection that applies uniform electric field between two metallic boundaries. The excitation at the port can be expressed as a voltage or a current. In this paper, we will use two lumped ports carrying an electrical current as a medium of excitation.

In this example, we consider a grounded coplanar waveguide that has three metallic plates running parallel to one another with two dielectric slabs attached in the center on top a dielectric substrate which is mounted on top of a metallic plate. Figure 8 shows the 2D cross-section of GCPW domain. We excite the grounded coplanar waveguide with running electric current in the x -direction. The domain has a symmetry in the y -direction, hence, we set $\frac{\partial}{\partial y}$ terms in Maxwell's 3D equations to 0. Simplifying, we use the TE model with electric field in the x and z direction, E_x , E_z and a magnetic field in the y -direction, H_y .

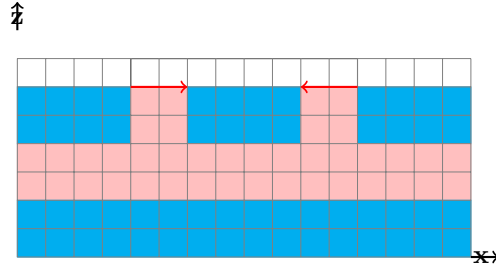


FIGURE 8. Three Metallic plates running parallel to one another with two Dielectric slabs attached in the center on top a dielectric substrate which is on top of a metallic plate along with current running in the x direction.

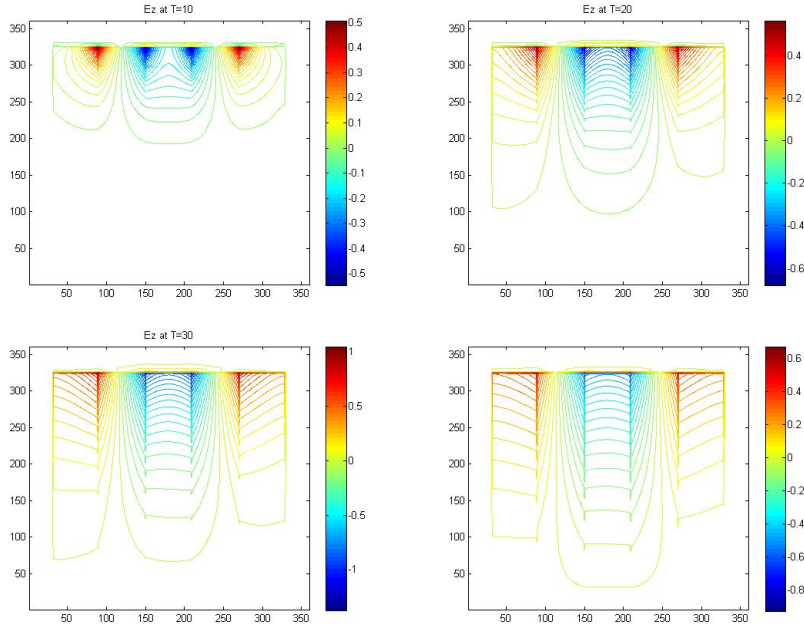


FIGURE 9. E_z at different times with $J_x = 10000 \sin(2\pi f_0 t)$ for the left current and $J_x = -10000 \sin(2\pi f_0 t)$ for the right side current.

Figure 9 shows the electric field in the z -direction for different times for current source dependent on time as stated in the figure. It shows that the electric field is stronger in the metal and weaker in the dielectric substrate. In the long run, the electromagnetic waves die out by the time it reaches the other side of the dielectric substrate. The figure makes it clear that the dielectric substrate slab is thick enough for the waves to become weak and die out and there is no electric current moving into the conductor at the bottom of the GCPW.

6.4. Transition between a Coplanar Waveguide and a Rectangular Waveguide. Now, we apply the EO-4th-EC scheme to the transition problem in [3]. The

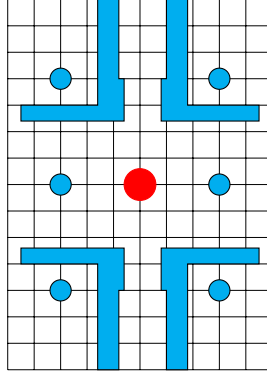


FIGURE 10. Cross section of transition between CPW and Rectangular Waveguide with source located in the center of the domain.

structure includes a rectangular waveguide synthesized with a linear array of metalized via holes on the same substrate used for the planar circuit as shown in Figure 1 in [3]. Such integrating structure reduces the size and cost. This structure is made of two back to back transitions from CPW to rectangular waveguide mounted on top same substrate layer. It consists of a coplanar waveguide with 90 degrees bend on each slot. A stub is added on the CPW lines to match the transition and the rectangular waveguide. However, the domain has been slightly modified to as seen in Figure 10. The same dimensions were used, however, less via metallic holes were considered to simplify the complex structure. In the experimental results concurred by paper [3], CPW was operated at a frequency of 19 to 38GHz and 27.5 to 29.5GHz provided the optimal result in terms of return loss. For this example, 28GHz is considered. The transition has a symmetry about the z -axis, hence, TE mode with E_x , E_y and H_z is used. The magnetic current source is added in the center of the domain as seen as red circle in Figure 10.

Figure 11 shows the contour figures of magnetic field in the z -direction for $T = 5, 10, 15, 20, 25$ and 27 . As time increases, the wave starts to move outwards towards the metallic stubs and the via holes. The dielectric substrate has a higher relative permittivity than the material used in the metals and holes. Hence, the electric field is stronger where there is a lower electric permittivity. The magnetic field is symmetric throughout the grid. Via holes are located near mesh points $(125, 125)$, $(125, 175)$, $(125, 275)$, $(275, 125)$, $(275, 175)$ and $(275, 275)$. In Figure 11, the bottom left picture show the magnetic field at the location of the holes at mesh point $(125, 175)$ and $(275, 175)$. When $T = 10$, the magnetic field hits the four corners and the wave starts to propagate differently. As the wave hits the holes, those sections are blue colour as seen in the last picture of Figure 11. Therefore, it shows that the waves move differently in different materials.

7. Conclusion

In this paper, we developed a new even-odd cycled energy-conserved splitting FDTD scheme to solve Maxwell's equations in 2D. The scheme is second order in time and fourth order in space. Theoretical analysis was done that the scheme is unconditionally stable, non-dissipative and energy conserved. Numerical experiments were computed using MATLAB codes to confirm that the scheme conserves

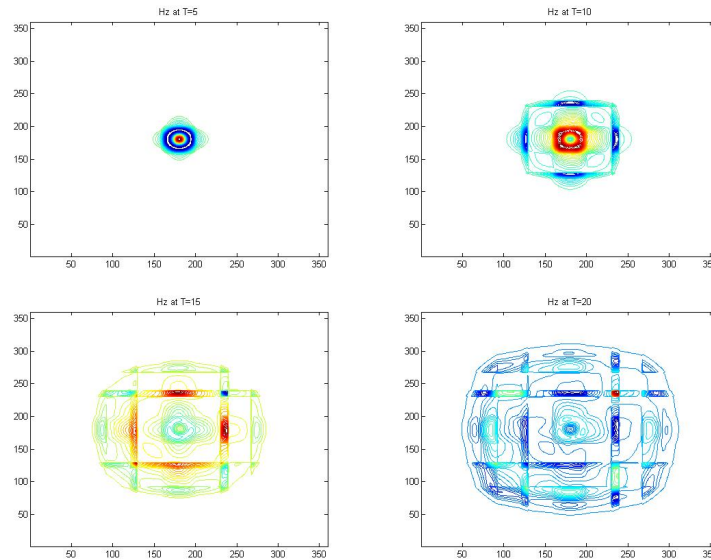


FIGURE 11. Propagations of H_z at $T = 5, 10, 15, 20, 25$ and 27 in the presence of via holes.

energy, and has high order accuracy in space and time. The approximation of divergence free has second order accuracy in time. The method was further used to compute the electromagnetic wave in a grounded coplanar waveguide as it propagates from dielectric material to metal layered conductors to the air in the distance between them. The method was also used to run a simulation for a transition domain between a rectangular waveguide and a coplanar waveguide.

Acknowledgement

This research was supported by the Natural Sciences and Engineering Research Council of Canada.

References

- [1] W. Chen, X. Li, D. Liang, Energy-conserved splitting FDTD methods for Maxwell's equations, *Numerische Mathematik*, 108 (2008), 445-485.
- [2] W. Chen, X. Li, D. Liang, Symmetric energy-conserved splitting FDTD scheme for the Maxwell's equations, *Commun. Comput. Phys.*, 6 (2009), 804-825.
- [3] D. Deslandes, K. Wu, Integrated transition of coplanar to rectangular waveguides, *Microwave Symposium Digest, 2001 IEEE MTT-S International*, Vol. 2. IEEE, (2001), 619-622.
- [4] T. Hirono, The second-order condition for the dielectric interface orthogonal to the Yee-lattice axis in the FDTD scheme, *IEEE microwave and guided wave letters*, 10 (2000), 359-361.
- [5] S. Hofschen, I. Wolff, Simulation of an elevated coplanar waveguide using 2-D FDTD, *IEEE Microwave and Guided Wave Letters*, 6 (1996), 28-30.
- [6] U. Inan, R. Marshall, *Numerical Electromagnetics; The FDTD Method*, Cambridge University, New York, 2011.
- [7] W. Li, D. Liang, Y. Lin, A new energy-conserved S-FDTD scheme for Maxwell's equations in metamaterials, *Int. J. Numer. Anal. Modelling*, 10 (2013), 775-794.
- [8] W. Li, D. Liang, The energy conservative splitting FDTD scheme and its energy Identities for metamaterial electromagnetic Lorentz system, *Comput. Phys. Commun.*, 239 (2019), 94-111.
- [9] D. Liang, Q. Yuan, The spatial fourth-order energy-conserved S-FDTD scheme for Maxwell's equations, *J. Comput. Phys.*, 243 (2013), 344-364.

- [10] G.C. Liang, Y.W. Liu, K.K. Mei, Full-wave analysis of coplanar waveguide and slotline using the time-domain finite-difference method, *IEEE Transactions Microwave Theory and Techniques*, 37 (1989), 1949-1957.
- [11] G.I. Marchuk, Splitting and Alternating Direction Methods, *Handbook of Numerical Analysis*. vol. 1, 1990.
- [12] P. Monk, E. Suli, A convergence analysis of Yee's scheme on nonuniform grids, *SIAM J. Numer. Anal.*, 31 (1994), 1056-1070.
- [13] T. Namiki, A new FDTD algorithm based on alternating-direction implicit method, *IEEE Transactions Microwave Theory and Techniques*, 47 (1999), 2003-2007.
- [14] A. Taflov, S. Hagness, *Computational Electromagnetics: The Finite Difference Time-Domain Method*, 2nd ed., Boston, MA: Artech House, 2000.
- [15] Z. Xie, C.H. Chan, B. Zhang., An explicit fourth-order staggered finite-difference time-domain method for Maxwell's equations, *J. Comput. Appl. Math.*, 147 (2002), 75-98.
- [16] N.N. Yanenko, *The Method of Fractional Steps*. New York: Springer-Verlag, 1971.
- [17] K.S. Yee, Numerical solution of initial boundary value problems involving Maxwell's equations in isotropic media, *IEEE Transactions on antennas and propagation*, 14 (1966), 302-307.
- [18] A.P. Zhao, Analysis of the numerical dispersion of the 2D alternating-direction implicit FDTD method, *IEEE Transactions on Microwave Theory and Techniques*, 50 (2002), 1156-1164.
- [19] F. Zheng, Z. Chen, J. Zhang, Toward the development of a three-dimensional unconditionally stable finite-difference time-domain method, *IEEE Transactions on Microwave Theory and Techniques*, 48 (2000), 1550-1558.

Department of Mathematics and Statistics, York University, Toronto, Ontario, M3J 1P3, Canada

E-mail: manindersarai89@gmail.com

Department of Mathematics and Statistics, York University, Toronto, Ontario, M3J 1P3, Canada

E-mail: dliang@yorku.ca